Experimental aspects of multiharmonic-order coherent diffractive imaging

Sven Teichmann,[1,a)] Bo Chen,[2] Ruben A. Dilanian,[2] Peter Hannaford,[1] and Lap Van Dao[1]
[1]*ARC Centre of Excellence for Coherent X-Ray Science, Centre for Atom Optics and Ultrafast Spectroscopy, Swinburne University of Technology, Melbourne 3122, Australia*
[2]*ARC Centre of Excellence for Coherent X-Ray Science, School of Physics, The University of Melbourne, Melbourne 3010, Australia*

(Received 21 April 2010; accepted 9 June 2010; published online 26 July 2010)

We describe some experimental aspects required for the implementation of a few-order high-harmonic source for coherent diffractive imaging in the extreme-ultraviolet region. Polychromatic high-angle diffractive images have been successfully processed for both periodic and aperiodic inorganic samples using a modified Gerchberg–Saxton algorithm and maximum-entropy-method refinement and reconstructions yielding a resolution of 100 nm can now be achieved at harmonic wavelengths around 32 nm. © *2010 American Institute of Physics*. [doi:10.1063/1.3462438]

I. INTRODUCTION

Since the first experiments in 1999 (Ref. 1) coherent diffractive imaging has developed into a well-established technique for determining the structure, shape and size of periodic and nonperiodic objects.[1–7] The use of extreme-ultraviolet or soft x-ray radiation from synchrotrons for high-resolution imaging has proven to be a promising approach and imaging in the so-called water-window of micrometer-thick samples and three-dimensional (3D) tomography at nanometer resolution has been achieved.[8–12] Coherent diffractive imaging can be applied to a range of objects, including both inorganic and biological samples, with the main limitation being radiation damage to the sample.

Femtosecond-laser based high-harmonic generation sources are increasingly being used for coherent diffractive imaging[13–15] to meet the increasing demand for high-resolution morphological and dynamical studies of nanometer-scale objects. Compared to synchrotrons, these table-top sources provide an output that exhibits a high degree of spatial coherence. In addition they are small-scale and highly versatile and their unique characteristics can be tailored to experimental requirements. However, by their nature, high-harmonic generation sources produce a laser-like beam consisting of multiple longitudinal coherent modes. Iterative methods[7] for image reconstruction inherently assume a fully coherent wave field. Thus, a single wavelength, corresponding to a single harmonic order, needs to be selected which leads to significantly reduced flux of the harmonic beam and longer acquisition times for the diffraction images.

Recently, we have demonstrated that a harmonic beam consisting of a few phase-matched harmonic orders generated in a semi-infinite gas cell can be utilized for high-quality sample reconstruction in coherent diffractive imaging.[14,15] The effective spectral range and the relative weights of the individual harmonic orders of the harmonic beam depend strongly on the focusing geometry and the macroscopic phase-matching parameters: by appropriate choice of species of gas and its pressure, the interaction geometry, the position of the laser focus in the gas cell and the intensity and diameter of the laser beam, the harmonic emission can be phase-matched and confined to just a few orders.[16–19] Thus, the orders of the harmonic beam can be tailored according to experimental requirements and all effectively available harmonic orders can be employed to keep the acquisition time short and to reduce sample damage or detrimental effects due to possible instabilities in the harmonic source. Furthermore, multiple-wavelength coherent diffractive imaging becomes a necessity when operating a high-harmonic source in the water-window (~2.3–4.4 nm) where the spacing of adjacent harmonic orders may become comparable or less than the spectral bandwidth of the wavelength-discriminating optical elements, such as a diffraction grating, used for selecting the harmonic orders.

We note that this high-harmonic source is a potential source of extreme-ultraviolet and soft x-ray radiation for time-resolved spectroscopy, such as femtosecond photoelectron spectroscopy, and for polychromatic diffractive imaging with high spatial resolution, where only a few harmonic orders of short wavelength or a dominant photon energy are required and any optics, such as reflection gratings, in the harmonic beam path, are undesirable. We note that the previously achieved resolution of ~165 nm in coherent diffractive imaging[14] was limited by the dynamic range of the acquired diffraction images, which did not permit detection of weak high-angle diffraction signals.

In this paper we discuss some experimental aspects to coherent diffractive imaging based on a few-order high-harmonic source. For a high-resolution output of the reconstruction process, and depending on the size of the sample and diameter of the harmonic beam, the sample may need to be used in combination with a micrometer-sized pinhole in order to define a precise area of illumination, to allow a high oversampling ratio, and to provide a support constraint for the reconstruction algorithm. We discuss the effect of such pinholes on the acquired diffraction images since they may introduce distortions to the diffraction data and thus affect the reconstruction. Employing a broad-bandwidth harmonic

a)Electronic mail: sventeichmann@swin.edu.au.

beam requires the use of x/y-beamstops in order to acquire images of dynamic range that exceed the natural dynamic range of the charged-couple device (CCD) and that are free from distortions and contributions of the supporting material of the beamstops for all harmonic wavelengths. We discuss the design of such x/y-beamstops and the methodology for acquiring high-quality diffraction images that capture the low-resolution and high-resolution features of the diffraction speckles. These images are then combined by a mathematical stitching procedure. Implementation of these procedures allows the acquisition of high-quality polychromatic high-angle diffractive images for both periodic and aperiodic inorganic samples. Using a modified Gerchberg–Saxton algorithm[20] and maximum-entropy-method refinement,[14,15] these images can then be reconstructed yielding a resolution of 100 nm.

II. GENERATION OF ONLY A FEW HIGH-HARMONIC ORDERS

The pump laser for the harmonic source is a 1 kHz multipass chirped-pulse amplifier system that produces 30 fs pulses centered at 805 nm. The unapertured and unfocused laser beam has a $1/e^2$-diameter of 12 mm and an energy of 2 mJ per pulse. Because of the chosen focal geometry and defocusing due to the intrinsic plasma generation, the effective focused intensity is $<3\times10^{14}$ W/cm^2. A calibrated aperture is applied to the laser beam before it is focused into a 260 mm long argon gas cell of pressure 58 Torr by a lens of focal length 400 mm. The pressure, aperture diameter, energy of the laser pulses, position of the laser focus relative to the exit of the gas cell, and chirping of the laser pulses are optimized in an iterative procedure for maximum flux of all available harmonics (21st to 31st) in the cutoff region This process allows us to effectively generate one to four intense harmonic orders around 30 nm, as shown in Fig. 1, with a high degree of spatial coherence and a good spatial profile[19] and to match the spectral characteristics of the harmonic beam with the transmissive characteristics of the sample.[14,15] The harmonic emission is confined to only a few orders due to a small phase mismatch in the cutoff region which allows phase-matching to be achieved by carefully choosing an appropriate focusing geometry and controlling the macroscopic phase-matching parameters.[16] We note that in this cutoff region the complex refractive indices related to refraction and absorption of the generating medium are large and depend strongly on the wavelength. It is this dependence that leads to the generation of only a few harmonics for certain experimental conditions and that allows the generation of these harmonic orders in a semi-infinite gas cell with a conversion efficiency that is much higher than when using a gas jet configuration.[16]

Spectral characterization of the harmonic emission is performed by a grazing incidence spectrometer (Setpoint GIMS #4) or by applying the maximum entropy method to the interference pattern of a Young double-slit pair illuminated with the emission from the harmonic source.[21] For the argon gas cell an aluminum metal filter is used to separate the harmonic emission from the fundamental laser beam. The sample for coherent diffractive imaging is mounted on x/y/z-translation stages and can be precisely moved into the multiple-order harmonic beam and at any distance in front of the center of the detector chip.[14,15] The diffracted emission of the sample after illumination with the broad-bandwidth harmonic beam is detected by a CCD with a 26.8×26.0 mm^2 chip of pixel size 20×20 μm^2 (Princeton Instruments PI-SCX 1340×1300 pixels) which is positioned 0.94 m from the exit of the gas cell.

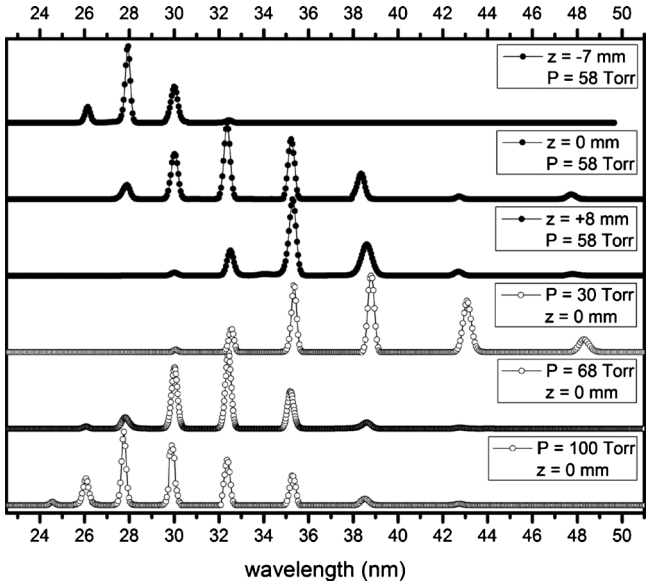

FIG. 1. Spectral tailoring: spectral characteristics of the harmonic beam depending on the macroscopic phase-matching parameters. Top (bottom) three curves: variation in the focal point position inside the gas cell z (pressure P) with constant pressure P (constant focal point position z). Global intensity maximum is at z=0 mm. The laser focus is close to the exit plane and deeper inside the gas cell for larger values of z for the position of maximum flux.

III. POLYCHROMATIC COHERENT DIFFRACTIVE IMAGING

Harmonic sources usually deliver a beam with diameter of the order of a few millimeters. If a micrometer-sized sample is to be investigated by coherent diffractive imaging, the beam needs to be focused onto the sample to a spot size that is comparable to the sample size. In this case the curvature of the field needs to be considered which can lead to difficulties in the reconstruction process especially when a broad band source is employed. Alternatively, a pinhole spatial filter can be employed to confine the area of illumination on the sample and to satisfy the requirement for oversampling. Furthermore, such a pinhole can provide the support constraint for the reconstruction algorithm. However, such a pinhole has the potential to severely distort the diffraction images depending on the quality of its edges. These distortions can be obvious when inorganic homogeneous periodic samples are investigated. However, in the case of organic inhomogeneous and aperiodic samples, such as biomolecules or clusters of molecules, the distortions can be hidden in and between the diffracted data and can severely hamper or even disrupt the recovery and reconstruction of the sample. The methodology and the algorithm of the reconstruction process are discussed extensively in Refs. 14 and 15. High-quality

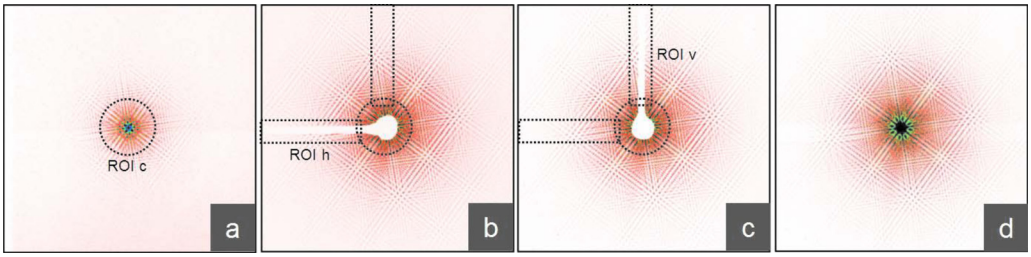

FIG. 2. (Color online) High-dynamic range diffraction images of the sample in Fig. 3: an image (a) of low-angle diffraction pattern and images [(b) and (c)] of high-angle diffraction patterns are acquired and stitched together to form a single image (d).

reconstructions could be achieved with experimental diffraction data from a high-harmonic generation source[14,15] but their resolution was limited by insufficient dynamic range of the data. We note that the pixel size or resolution of the reconstructed image is proportional to the size of the sample convoluted with the size of the illuminated area and depends on the wavelength of the illuminating radiation, the distance between the sample and the detector and the number and size of the pixels in the CCD.

A. High-dynamic range diffractive imaging

Implementing a beamstop adaptor allows the acquisition of diffraction patterns over a dynamic range that exceeds the natural dynamical range of the CCD detector chip which is necessary in order to capture the high-angle high-resolution diffraction features. As shown in Fig. 2, three different diffraction patterns of the same sample (shown in Fig. 3) are taken with special emphasis on the diffractive features in the center [panel (a) of Fig. 2] and in the wings of the diffraction pattern [panels (b) and (c) of Fig. 2]. For the latter, longer exposure times are needed in order to resolve the features with a reasonable signal-to-noise ratio. Saturation of the center features in the acquired image is avoided by placing a beam stop over the center of the CCD detector chip. This is done independently for the x-[frame (b) of Fig. 2] and y-direction [frame (c) of Fig. 2]. The three diffraction images are then combined [frame (d) of Fig. 2]. This technique allows the acquisition of high-dynamic range diffraction patterns that exceed the natural dynamic range of the detector chip by a factor of ~100, or higher if necessary, and that are free from any diffraction or shadows from elements of the beam block, such as very thin wires that support the beam block. We note that the simpler approach of using two crossed thin wires with a beam block at their crossing might not be applicable when a harmonic beam of multiple orders is employed because it may be difficult or impossible to find a material of suitable thickness for the wires that is transparent to all wavelengths.

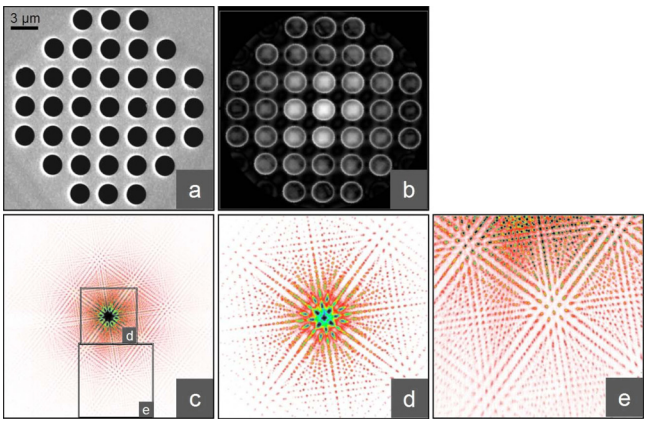

FIG. 3. (Color online) Microscopic periodic sample: scanning electron microscopy image (a), reconstructed image (b), diffraction pattern (c), and zoom into low-diffraction angle and high-diffraction angle regions [(d) and (e)].

Prior to acquisition of the diffraction images the broadbandwidth harmonic source is optimized and characterized with respect to its intensity and spatial characteristics by adjusting the macroscopic phase-matching parameters[16–19] and analyzing its spectral characteristics.[21] For the latter and for the required input of the reconstruction algorithm an interference pattern of high-dynamic range from a Young double-slit pair is taken. This *in situ* spectral characterization allows the spectral power distribution to be matched with respect to the transmissive characteristics of the sample by adjusting the macroscopic phase-matching parameters. The sample is now positioned so that the center of the diffraction pattern coincides with the center of the detector. Then the signal images [panels (a)–(c) in Fig. 2] are taken; each signal image is followed by its background image which is taken with the gas cell vented and with the x- or y-beamstop in the same location. The background images are dominated by thermal and readout noise, and any scattered fundamental laser light can be neglected. This is due to carefully chosen aluminum metal filters that separate the harmonic emission from the highly divergent fundamental laser light and due to a light shield that has been installed in front of the sample. The main part of the light shield is an aperture of large diameter (~mm) that, if needed, can be adjusted to block any remaining scattered laser light.

The low-angle diffraction image [panel (a) in Fig. 2] and the two high-angle diffraction images [panels (b) and (c) in Fig. 2] need to be stitched together to form a high-dynamic range diffraction image to which the reconstruction algorithm can be applied. In order to smoothly stitch together the information from these images, a region somewhat larger than ROI c, ROI h, and ROI v [panels (a)–(c) in Fig. 2] is chosen and the data sets are weighted using the expression

$$I = (1 - G)I_{ROI\,c} + G[(1 - F)I_{ROI\,h} + F\ I_{ROI\,v}],$$

where $I_{ROI\,c}$ is the data from the region of interest ROI c of Fig. 2, $I_{ROI\,h(v)}$ is the data from the panels (b) and (c) with the

missing data from ROI h(v), and F and G are the Gaussian coefficient functions

$$F = \exp(-r_F^2/2\sigma_F^2), \quad G = \exp(-r_G^2/2\sigma_G^2),$$

where

$$r_F = \begin{cases} |y-y_0|, & \text{if } r \geq R_F \\ 0, & \text{otherwise} \end{cases}$$

and

$$r_G = \begin{cases} |x^2+y^2|, & \text{if } r \geq R_G \\ 0, & \text{otherwise} \end{cases},$$

where x, y, y_0, r, R_G, and R_F are spatial coordinates referring to the x- and y-direction and the spatial dimensions of ROI c, ROI h, and ROI v.

B. Diffractive imaging of a periodic sample

A scanning electron microscopy image of a microscopic periodic sample is shown in panel (a) of Fig. 3. The sample is a Si_3N_4 substrate coated with a thin ($\geq$100 nm) gold layer in which a periodic array of pinholes 2 μm diameter and 3 μm spacing has been fabricated. Panel (c) shows the diffraction pattern of this sample and a zoom into the low-diffraction angle region (1 s exposure time) and high-angle diffraction region (135 s exposure time) is shown in panels (d) and (e). The reconstruction of this diffraction pattern based on a multiple-order harmonic beam is shown in panel (b) and yields a resolution of 100 nm (full width at half maximum). A Fresnel transform has been employed in this case as the far-field condition was not met. The size of each pixel within a reconstructed image is determined by a trade-off of several experimental parameters. In order to achieve a desired theoretical resolution of the reconstructed image,[15] and for a given illumination wavelength and parameters of the detector, a balance between the propagation length of the diffracted signal and the diameter of the sample has to be found. This is due to the limitations based on the requirements related to the Fraunhofer criterion and oversampling ratio.[1] The resolution is determined by fitting a sigmoid to the edge distribution of the individual pinholes in the reconstructed image and is consistent with a simulated value of $\Delta = 0.94\ \lambda_c/\mathrm{NA} \approx 100$ nm based on the Sparrow criterion, where the center wavelength of the polychromatic harmonic beam is $\lambda_c = 32.2$ nm, and NA$\approx$0.29 is given by the sine of the vertex angle for the largest cone of meridional rays that can enter the CCD chip. We note that the achieved resolution is considerably better than the resolution ($\sim$165 nm) previously published in Ref. 14 due to implementation of the independent x/y-beamstop design described in Sec. III A. Thus, the dynamic range of the acquired diffraction images is $\sim 7 \times 10^6$ which is $\sim$100 times larger than the 16 bit dynamic range of the detector.

It is apparent that the algorithm fits a nonzero intensity inside the individual pinholes of the array and even fits extremely weak intensity pinholes outside the array of pinholes. The origin of this artifact could be due to an imbalance of the reconstruction by the modified Gerchberg–Saxton iteration and the image quality refinement by the maximum entropy method. The fact that the algorithm overestimates the level of noise in the reconstructed image and probably underfits the data can be seen and is discussed in our previous work.[14]

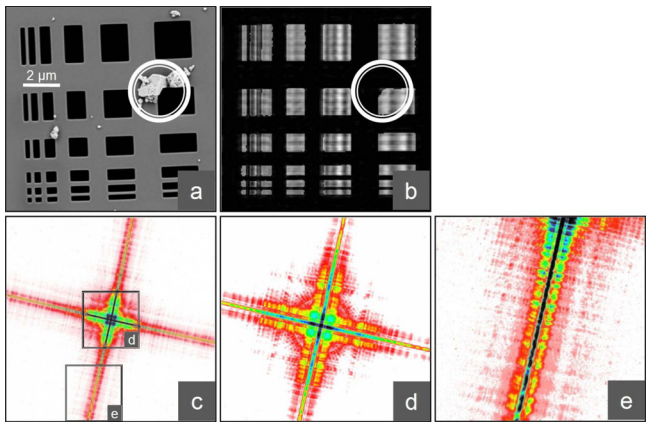

FIG. 4. (Color online) Microscopic aperiodic sample: scanning electron microscopy image (a), reconstructed image (b), diffraction pattern (c), and zoom into low-diffraction angle and high-diffraction angle regions [(d) and (e)].

C. Diffractive imaging of an aperiodic sample

The polychromatic reconstruction algorithm[14,15] can successfully handle the processing of microscopic samples of periodic nature, e.g., a periodic array of pinholes, irrespective of whether the sample transmission function depends on the spectral bandwidth of the harmonic beam. This also holds for a microscopic sample of aperiodic nature, e.g., an ensemble of rectangular pinholes of different sizes. A scanning electron microscopy image of such a sample is shown in panel (a) of Fig. 4. This sample is a Si_3N_4 substrate coated with a thin ($\geq$100 nm) gold layer in which a square array of size 10×10 μm^2 with rectangular pinholes of different lengths and widths has been fabricated. Panel (c) shows the diffraction pattern of this sample, and a zoom into the low-diffraction angle region (3 s exposure time) and high-angle diffraction region (300 s exposure time) is shown in panels (d) and (e). The reconstruction of this diffraction pattern based on a multiple-order harmonic beam is shown in panel (b) and yields a resolution of 100 nm (full width at half maximum), which is consistent with the simulated value of 100 nm based on the Sparrow criterion (see Sec. III B). The dynamic range of the acquired diffraction images is $\sim 3 \times 10^6$ which is $\sim$50 times larger than the 16 bit dynamic range of the detector.

Clearly, the algorithm can recover the rectangular pinholes of different lengths and widths from the diffraction pattern as shown in panel (b) of Fig. 4. Moreover, as indicated by the white circle in panels (a) and (b), the algorithm even recovers a contamination particle on the edge of one of the rectangular pinholes. It is apparent that each of the rectangular pinholes exhibits faint cross-like structures that probably have the same or a related origin. A similar effect is observed in our previous work[14] and was discussed in Sec. III B.

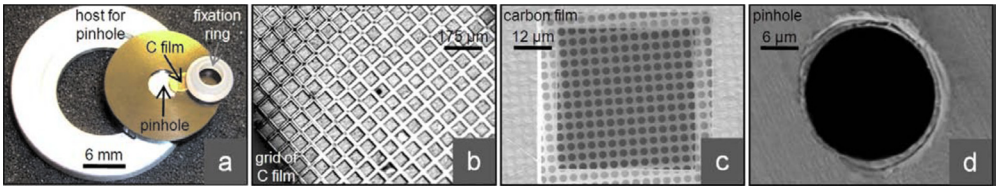

FIG. 5. (Color online) Macroscopic sample: carbon film mounted in a sandwich structure (a); copper support grid of the nanometer-carbon film (b), and carbon film mounted on that grid (c); 20 μm diameter pinhole to confine the area of illumination (d).

D. Diffractive imaging of a composite sample consisting of a pinhole and a microscopic periodic sample

We now compare the microscopic sample from Fig. 3 with a macroscopic periodic sample, which is shown in Fig. 5 and has been investigated extensively in Ref. 14 by coherent diffractive imaging based on a broad-bandwidth harmonic source. As shown in panel (a) the carbon film is mounted on a commercial precision pinhole by means of a fixation ring and attached to a metal ring which is part of the system that carries the sample and controls its position with respect to the harmonic beam and the center of the detector. In contrast to the sample in Fig. 3 a micrometer-sized pinhole needs to be employed to restrict the area of illumination, to satisfy the requirement for oversampling and high-resolution reconstruction images, and also to provide a support constraint for the reconstruction algorithm. The carbon film is ~40 nm thick and mounted on a copper grid as shown in panel (b). A zoom into this picture shows a small part of the sample lying on the copper grid as shown in panel (c): the carbon film exhibits an array of pinholes with diameter 2 μm and spacing 3 μm. Panel (d) shows the 20 μm diameter and 13 μm thick commercial precision pinhole used to define the area of the carbon film illuminated by the multiple-order harmonic beam. Coherent diffractive imaging of this sample has been discussed extensively in Ref. 14.

E. Effect of pinholes on diffractive images

The diffraction image of the macroscopic periodic sample in combination with a pinhole in Fig. 5 is shown in our previous paper:[14] small cloudy distortions are observed that are considerably smaller than the diffraction speckles in the same regions of the diffraction image. In this case the cutoff level for the background can be adjusted depending on the radial position and the reconstruction algorithm can successfully recover the sample[14,15] and yields a resolution of ~165 nm. Depending on the quality of the edges of the pinhole throughout its thickness, these distortion effects can be negligible or prominent. Although the edges of the inner part of the pinhole in panel (a) of Fig. 6 appear to be reasonably smooth, and in comparison with the pinhole in panel (a) of Fig. 6, it is clear that the overall structure is rather complex. Investigating the diffraction pattern in panel (b) reveals strong distortions compared to the expected diffracted image of a perfect pinhole. In panel (c) the harmonic beam first passes the pinhole and then the carbon film. The diffraction features of the pinhole dominate the diffraction features of the carbon film and, in particular, three regions of high-intensity features (dotted ellipses) can be seen that spatially coincide with the regions marked by dotted ellipses in panel (b). In panel (d) the harmonic beam first passes the carbon film and then the pinhole. Here, the diffractive features of the carbon film dominate and a radial ray structure can be seen. The intensity of these rays is small compared with the intensity of the central diffraction features of the carbon film, but large compared with the high-angle diffraction features at the edges of the CCD detector chip. We note that in both cases, as shown in panels (c) and (d) of Fig. 6, the modified Gerchberg–Saxton iteration, as discussed in Refs. 14 and 15 was not able to recover the morphology of the carbon film sample. In the case shown in panel (d) of Fig. 6 the contributions of the pinhole are not necessarily obvious [compare with panel (c) of Fig. 3]: if inhomogeneous and aperiodic samples are investigated, such as biomolecules or clusters of molecules, these distortions may remain unnoticed as they are hidden in and between the diffracted data and thus can severely hamper or even completely disrupt the recovery and reconstruction of the sample.

In most cases it is impossible to make a reference measurement of the diffraction pattern of the pinhole without the sample and to subtract the diffracted information of the pinhole edges from the diffraction image of the sample plus the pinhole. A slightly different position of the pinhole (and its complex internal structure) or the orientation of the sample with respect to the sample itself will inevitably affect the contributions to the diffraction pattern. However, by carefully investigating the diffraction pattern of the pinhole under different experimental conditions and at slightly different locations and orientations with respect to the sample one can estimate the effect of the pinhole on the diffraction pattern of the sample. Employing focused ion beam etching, which allowed us to manufacture the periodic and aperiodic samples, can be used to produce pinholes with edges of very high-quality (see Figs. 4 and 5). We find that these pinholes are superior to commercial pinholes that have been manufactured by laser ablation.

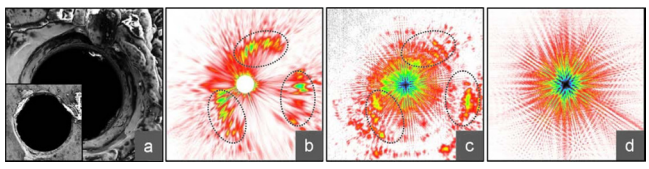

FIG. 6. (Color online) Distortions in the diffraction images: complex structure of the mounted pinhole on both sides (a); diffraction pattern of the pinhole itself (b); harmonic beam illuminates the pinhole first, then carbon film (c); and harmonic beam illuminates the carbon film first, then the pinhole (d).

IV. CONCLUSIONS

We have discussed some experimental aspects of employing a broad-bandwidth extreme-ultraviolet harmonic beam for coherent diffractive imaging. Use of a micrometer-sized pinhole in combination with the sample for coherent diffractive imaging may be necessary depending on the geometry of the sample and the spatial extent of the harmonic beam in order to restrict the area of illumination and to achieve a high-resolution of the reconstructed image of the sample. The edges and the complex 3D structure of such a pinhole can introduce obvious or hidden distortions in the diffraction image depending on the nature of the sample and the order of the pinhole and the sample. Knowledge of the effects of the pinhole on the diffraction image of the sample is essential in order to achieve a high-quality reconstruction of the sample. We have discussed a novel design of x/y-beamstops for the acquisition of short-exposure low-angle diffraction and long-exposure high-angle diffraction images which is often necessary when employing a broad-bandwidth harmonic source. The design of this beamstop involves the acquisition of a number of different diffraction images that need to be combined. We have described a stitching process in which the images are combined by applying Gaussian coefficient functions to chosen regions with diffraction speckles. Such combined high-dynamic range polychromatic diffraction images of periodic and aperiodic inorganic samples can then be successfully processed iteratively by a modified Gerchberg–Saxton algorithm and lead to reconstructions yielding a resolution of 100 nm at harmonic wavelengths centered at 32 nm.

ACKNOWLEDGMENTS

The authors acknowledge support from the Australian Research Council and the Victorian government Strategic Technology Innovation initiative. The authors thank Dr. Eugeniu Balaur at La Trobe University for providing the Young double-slit pair and the mirofabricated periodic and aperiodic samples.

[1] J. Miao, P. J. Miao, P. Charalambous, J. Kirz, and D. Sayre, Nature (London) **400**, 342 (1999).
[2] I. K. Robinson, I. A. Vartanyants, G. J. Williams, M. A. Pfeifer, and J. A. Pitney, Phys. Rev. Lett. **87**, 195505 (2001).
[3] J. Miao, T. Ishikawa, B. Johnson, E. H. Anderson, B. Lai, and K. O. Hodgson, Phys. Rev. Lett. **89**, 088303 (2002).
[4] G. J. Williams, H. M. Quiney, B. B. Dhal, C. Q. Tran, K. A. Nugent, A. G. Peele, D. Paterson, and M. D. de Jonge, Phys. Rev. Lett. **97**, 025506 (2006).
[5] C. G. Schroer, P. Boye, J. M. Feldkamp, J. Patommel, A. Schropp, A. Schwab, S. Stephan, M. Burghammer, S. Schöder, and C. Riekel, Phys. Rev. Lett. **101**, 090801 (2008).
[6] J. R. Fienup, Appl. Opt. **21**, 2758 (1982).
[7] J. R. Fienup, Opt. Lett. **3**, 27 (1978).
[8] D. Attwood, *Soft X-Rays and Extreme Ultraviolet Radiation*, 1st ed. (Cambridge University Press, New York, 1999).
[9] C. A. Larabell and M. A. Le Gros, Mol. Biol. Cell **15**, 957 (2004).
[10] S. Eisebitt, J. Lüning, W. F. Schlotter, M. Lörgen, O. Hellwig, W. Eberhardt, and J. Stöhr, Nature (London) **432**, 885 (2004).
[11] P. Fischer, D.-H. Kim, W. Chao, J. A. Liddle, E. H. Anderson, and D. T. Attwood, Mater. Today **9**, 26 (2006).
[12] D. Sayre, J. Kirz, R. Feder, D. M. Kim, and E. Spiller, Ultramicroscopy **2**, 337 (1976).
[13] A. Rundquist, C. G. Durfee III, Z. Chang, C. Herne, S. Backus, M. M. Murnane, and H. C. Kapteyn, Science **280**, 1412 (1998).
[14] B. Chen, R. D. Dilanian, S. Teichmann, B. Abbey, A. G. Peele, G. J. Williams, P. Hannaford, L. Van Dao, H. M. Quiney, and K. A. Nugent, Phys. Rev. A **79**, 023809 (2009).
[15] R. A. Dilanian, B. Chen, G. J. Williams, H. M. Quiney, K. A. Nugent, S. Teichmann, P. Hannaford, L. Van Dao, and A. G. Peele, J. Appl. Phys. **106**, 023110 (2009).
[16] L. Van Dao, S. Teichmann, J. Davis, and P. Hannaford, J. Appl. Phys. **104**, 023105 (2008).
[17] L. Van Dao, S. Teichmann, and P. Hannaford, Phys. Lett. A **372**, 5254 (2008).
[18] S. Teichmann, P. Hannaford, and L. Van Dao, Appl. Phys. Lett. **94**, 171111 (2009).
[19] S. Teichmann, B. Chen, R. A. Dilanian, P. Hannaford, and L. Van Dao, J. Phys. D: Appl. Phys. **42**, 135108 (2009).
[20] R. W. Gerchberg and W. O. Saxton, Optik (Stuttgart) **35**, 237 (1972).
[21] R. D. Dilanian, B. Chen, H. M. Quiney, K. A. Nugent, S. Teichmann, and L. Van Dao, Opt. Lett. **33**, 2341 (2008).